Available online at www.sciencedirect.com
SCIENCE DIRECT®
APPLIED MATHEMATICS AND COMPUTATION
ELSEVIER Applied Mathematics and Computation 175 (2006) 902–922
www.elsevier.com/locate/amc

Numerical simulation of rotating accretion disk around the Schwarzschild black hole using GRH code

Orhan Dönmez

Nigde University, Faculty of Art and Science, Physics Department, 51200 Nigde, Turkey

Abstract

The 2D time dependent solution of thin accretion disk in a close binary system have been presented on the equatorial plane around the Schwarzschild black hole. To do that, the special part of the general relativistic hydrodynamical (GRH) equations are solved using high resolution shock capturing (HRSC) schemes. The spiral shock waves on the accretion disk are modeled using perfect fluid equation of state with adiabatic indices $\gamma = 1.05$, 1.2 and 5/3. The results show that the spiral shock waves are created for gammas except the case $\gamma = 5/3$. These results are consistent with the results from Newtonian hydrodynamic code except those which are close to black hole. Newtonian approximation does not give good solution when the matter is close to the black hole. Our simulations illustrate that the spiral shock waves are created close to black hole and the location of inner radius of spiral shock wave is around $6M$ and it depends on the specific heat rates. We also find that the smaller γ is the more tightly packed in the spiral winds.

Keywords: General relativity; Hydrodynamics; Numerical relativity black hole; Accretion disk; Spiral shock; Adaptive-mesh refinement

E-mail address: odonmez@nigde.edu.tr

0096-3003/$ - see front matter
doi:10.1016/j.amc.2005.08.009

1. Introduction

Rotating accretion disk around compact objects is an important problem in astrophysics, such as neutron stars and black holes which involve mass transfer from one object to another. Shock waves in a rotating accretion disk onto compact objects transfer the gravitation energy to the radiation energy which is observed by different X-ray observatory satellite, such as Chandra. Fluctuations and oscillations of radiation emitted from these systems constantly remind us of time variations of the dynamical quantities. These variations can occur on times scale for a few microseconds to few years. In order to understand these kinds of events we have started doing some numerical simulation and looking for shock waves on an accretion disk.

In binary systems in which a compact primary star accretes, through an accretion disc from a lobe-filling secondary star, the tidal interaction with the companion can result in the formation of a two-armed spiral structure [4,8]. These spiral waves can transport angular momentum in the accretion disk which has been suggested by analogy to the galactic dynamics context [13].

The problem of accretion disk on to black hole has been previously analyzed numerically by Hawley et al. [9] in general relativity. They also suggested shock waves on the rotating accretion disk. After that, many astrophysicists worked on this kind of problem using Newtonian (pseudo-Newtonian gravitational potential approximation) and general relativistic hydrodynamics. In the works of Chakabarti and Molteni [2], they compared the analytic and numerical studies of shock wave on inviscid accretion disk flows using the smoothed particle hydrodynamics (SPH) code. They believed that shock waves could be common in accretion disk and standing shock waves can only be produced in accretion disk around the black hole. Near to the black hole, density of accretion disk in the sub-Keplerian flows is higher than the density of accretion disk in Keplerian flows due to the consequence of the presence of centrifugal barrier, which is smaller at sub-Keplerian flow. Because of this high density, standing shock waves can form in the accretion disk. This high density flow intercepts soft photons from a cold Keplerian disk and reprocesses them to form high energy X-rays [3]. In the works of Lanzafame et al. [10], they have used SPH code with viscosity to look at the shock waves on an accretion disk at parameter range. They found that if viscosity parameter is less than critical values, shock can be formed. If it is bigger than critical values, shock wave disappears. In the intermediate viscosity, the disk oscillates in the viscous time scales. Non-axisymmetric shock waves are found on the equatorial plane by Molteni et al. [12]. They used SPH and Eulerian type with TVD codes to look for non-axisymmetric shock wave, applying a perturbation on an accretion disk at different parameter range, which are specific angular momentum and internal energy. They concluded that the shock waves found by Chakabarti with perturbation in a rotating inviscid accretion flow are generally unstable to azimithual

perturbation, but the instability are taken care of at low level and new stable asymmetric accretion disk is developed with a strong shock rotating steadily.

In the works of Makita et al. [11], first, they reviewed the spiral shock wave in 2D and 3D, and showed their results to look for consistency with the literature. The main problem in accretion disk is the mechanism of angular momentum transport. One of the reason for angular momentum transport is α-disk model. The viscosity is supposed to transform the angular momentum and it can produce shock waves depending on the parameter. Another way of the transporting angular momentum is the spiral shock waves. The first convincing evidence of spiral shock wave in an accretion disk is observed by Steeghs et al. [15]. They used the technique which is known as Doppler temography to observe spiral structure in the accretion disk of the eclipsing dwarf nova binary IP Peg at the outburst phase.

Here we do perturbation onto spherically symmetric steady state accretion disk around the black hole. Most of the numerical calculations for accretion disk are done by Newtonian hydrodynamical code using relativistic approximation on it. But our code fully inviscid general relativistic hydrodynamical which is used high resolution shock capturing scheme (HRSC). General relativistic code gives us more detailed explanations when the fluid flows closer to the black hole.

2. Formulation

The GRH equations in Refs. [7,5], written in the standard covariant form, consist of the local conservation laws of the stress-energy tensor $T^{\mu\nu}$ and the matter current density J^{μ}:

$$\nabla_{\mu} T^{\mu\nu} = 0, \quad \nabla_{\mu} J^{\mu} = 0. \tag{1}$$

Greek indices run from 0 to 3, Latin indices from 1 to 3, and units in which the speed of light $c = 1$ are used.

Defining the characteristic waves of the general relativistic hydrodynamical equations is not trivial with imperfect fluid stress-energy tensor. We neglect the viscosity and heat conduction effects. This defines the perfect fluid stress-energy tensor. We use this stress-energy tensor to derive the hydrodynamical equations. With this perfect fluid stress-energy tensor, we can solve some problems which are solved by the Newtonian hydrodynamics with viscosity, such as those involving angular momentum transport and shock waves on an accretion disk, etc. Entropy for perfect fluid is conserved along the fluid lines. The stress energy tensor for a perfect fluid is given as

$$T^{\mu\nu} = \rho h u^{\mu} u^{\nu} + P g^{\mu\nu}. \tag{2}$$

A perfect fluid is a fluid that moves through spacetime with a 4-velocity u^{μ} which may vary from event to event. It exhibits a density of mass ρ and isotro-

pic pressure P in the rest of the frame of each fluid element. h is the specific enthalpy, defined as

$$h = 1 + \epsilon + \frac{P}{\rho}. \tag{3}$$

Here ϵ is the specific internal energy. The equation of state might have the functional form $P = P(\rho, \epsilon)$. The perfect gas equation of state,

$$P = (\Gamma - 1)\rho\epsilon \tag{4}$$

is such a functional form.

The conservation laws in the form given in Eq. (1) are not suitable for the use in advanced numerical schemes. In order to carry out numerical hydrodynamic evolutions such as those reported in [7], and to use HRSC methods, the hydrodynamic equations after the $3 + 1$ split must be written as a hyperbolic system of the first order flux conservative equations. We write Eq. (1) in terms of coordinate derivatives, using the coordinates $(x^0 = t, x^1, x^2, x^3)$. Eq. (1) is projected onto the basis $\{n^\mu, (\frac{\partial}{\partial x^i})^\mu\}$, where n^μ is a unit timelike vector normal to a given hypersurface. After a straightforward calculation, we get (see [7]),

$$\partial_t \vec{U} + \partial_i \vec{F}^i = \vec{S}, \tag{5}$$

where $\partial_t = \partial/\partial t$ and $\partial_i = \partial/\partial x^i$. This basic step serves to identify the set of unknowns, the vector of conserved quantities $\vec{U}$, and their corresponding fluxes $\vec{F}(\vec{U})$. With the equations in conservation form, almost every high resolution method devised to solve hyperbolic systems of conservation laws can be extended to GRH.

The evolved state vector $\vec{U}$ consists of the conservative variables (D, S_j, τ) which are conserved variables for density, momentum and energy, respectively; in terms of the primitive variables (ρ, v^i, ϵ), this becomes [7]

$$\vec{U} = \begin{pmatrix} D \\ S_j \\ \tau \end{pmatrix} = \begin{pmatrix} \sqrt{\gamma} W \rho \\ \sqrt{\gamma} \rho h W^2 v_j \\ \sqrt{\gamma}(\rho h W^2 - P - W\rho) \end{pmatrix}. \tag{6}$$

Here, γ is the determinant of the 3-metric γ_{ij}, v_j is the fluid 3-velocity, and W is the Lorentz factor,

$$W = \alpha u^0 = (1 - \gamma_{ij} v^i v^j)^{-1/2}. \tag{7}$$

The flux vectors $\vec{F}^i$ are given by Font et al. [7]

$$\vec{F}^i = \begin{pmatrix} \alpha(v^i - \frac{1}{\alpha}\beta^i) D \\ \alpha\left\{ (v^i - \frac{1}{\alpha}\beta^i) S_j + \sqrt{\gamma} P \delta^i_j \right\} \\ \alpha\left\{ (v^i - \frac{1}{\alpha}\beta^i)\tau + \sqrt{\gamma} v^i P \right\} \end{pmatrix}. \tag{8}$$

The spatial components of the 4-velocity u^i are related to the 3-velocity by the following formula: $u^i = W(v^i - \beta^i/\alpha)$. α and β^i are the lapse function and the shift vector of the spacetime, respectively. The source vector $\vec{S}$ is given by Font et al. [7]

$$\vec{S} = \begin{pmatrix} 0 \\ \alpha\sqrt{\gamma}T^{\mu\nu}g_{\nu\sigma}\Gamma^{\sigma}_{\mu j} \\ \alpha\sqrt{\gamma}(T^{\mu 0}\partial_{\mu}\alpha - \alpha T^{\mu\nu}\Gamma^{0}_{\mu\nu}) \end{pmatrix}, \tag{9}$$

where $\Gamma^{\alpha}_{\mu\nu}$ is the 4-dimensional Christoffel symbol

$$\Gamma^{\alpha}_{\mu\nu} = \frac{1}{2}g^{\alpha\beta}(\partial_{\mu}g_{\nu\beta} + \partial_{\nu}g_{\mu\beta} - \partial_{\beta}g_{\mu\nu}). \tag{10}$$

The numerical solution of general relativistic hydrodynamical equations and technique used are explained in detail in our first paper Dönmez [6] which gives great detail about formulations, numerical scheme, technique, numerical solution of GRH equations, adaptive-mesh refinement (AMR) and solution of special relativistic test problem.

3. General relativistic hydrodynamical test problem

In this section, the Schwarzschild geometry is introduced in spherical coordinates to define sources for the general relativistic hydrodynamical equations. Then the accretion disk problems are numerically modeled, which have been analytically analyzed, to test the full GRH code in 2D in the equatorial plane.

3.1. Schwarzschild black hole

The Schwarzschild solution determined by the mass M gives the geometry in outside of a spherical star or black hole. The Schwarzschild spacetime metric in spherical coordinates is

$$\mathrm{d}s^2 = -\left(1 - \frac{2M}{r}\right)\mathrm{d}t^2 + \left(1 - \frac{2M}{r}\right)^{-1}\mathrm{d}r^2 + r^2\,\mathrm{d}\theta^2 + r^2\sin^2\theta\,\mathrm{d}\phi^2. \tag{11}$$

It behaves badly near $r = 2M$; there the first term becomes zero and the second term becomes infinite in Eq. (11). That radius $r = 2M$ is called the Schwarzschild radius or the Schwarzschild horizon.

The lapse function and shift vector for this metric is

$$\beta^r = 0.0, \quad \beta^{\theta} = 0.0, \quad \beta^{\phi} = 0.0,$$
$$\alpha = \left(1 - \frac{2M}{r}\right)^{1/2}. \tag{12}$$

3.2. The source terms for Schwarzschild coordinates

The gravitational sources for the GRH equations are given by Eq. (9). In order to compute the sources in Schwarzschild coordinates for different conserved variables, Eq. (9) can be rewritten as

$$\vec{S} = \begin{pmatrix} 0 \\ \alpha\sqrt{\gamma}T^{\mu\nu}g_{\nu\sigma}\Gamma^{\sigma}_{\mu r} \\ \alpha\sqrt{\gamma}T^{\mu\nu}g_{\nu\sigma}\Gamma^{\sigma}_{\mu\theta} \\ \alpha\sqrt{\gamma}T^{\mu\nu}g_{\nu\sigma}\Gamma^{\sigma}_{\mu\phi} \\ \alpha\sqrt{\gamma}(T^{\mu 0}\partial_{\mu}\alpha - \alpha T^{\mu\nu}\Gamma^{0}_{\mu\nu}) \end{pmatrix}. \tag{13}$$

It is seen in Eq. (9) that the source for conserved density, D, is zero but the other sources depend on the components of the stress energy tensor, Christoffel symbols, and 4-metric. After doing some straightforward calculations, the sources can be rewritten in Schwarzschild coordinates for each conserved variable with the following form:

The source for the momentum equation in the radial direction is

$$\alpha\sqrt{\gamma}T^{\mu\nu}g_{\nu\sigma}\Gamma^{\sigma}_{\mu r} = \frac{1}{2}\alpha\sqrt{\gamma}(T^{tt}\partial_r g_{tt} + T^{rr}\partial_r g_{rr} + T^{\theta\theta}\partial_r g_{\theta\theta} + T^{\phi\phi}\partial_r g_{\phi\phi}). \tag{14}$$

The source for the momentum equation in the θ direction is

$$\alpha\sqrt{\gamma}T^{\mu\nu}g_{\nu\sigma}\Gamma^{\sigma}_{\mu\theta} = \frac{1}{2}\alpha\sqrt{\gamma}T^{\phi\phi}\partial_{\theta}g_{\phi\phi}. \tag{15}$$

The source for the momentum equation in the ϕ direction is

$$\alpha\sqrt{\gamma}T^{\mu\nu}g_{\nu\sigma}\Gamma^{\sigma}_{\mu\phi} = 0.0. \tag{16}$$

The source for the energy equation is

$$\alpha\sqrt{\gamma}(T^{\mu 0}\partial_{\mu}\alpha - \alpha T^{\mu\nu}\Gamma^{0}_{\mu\nu}) = \alpha\sqrt{\gamma}(T^{rt}\partial_r\alpha - \alpha T^{rt}g^{tt}\partial_r g_{tt}). \tag{17}$$

The non-zero components of the stress-energy tensor in Schwarzschild coordinates which can be computed by Eq. (2); they are

$$\begin{aligned} T^{tt} &= \rho h\frac{W^2}{\alpha^2} + Pg^{tt}, \\ T^{rr} &= \rho h W^2(v^r)^2 + Pg^{rr}, \\ T^{\theta\theta} &= \rho h W^2(v^{\theta})^2 + Pg^{\theta\theta}, \\ T^{\phi\phi} &= \rho h W^2(v^{\phi})^2 + Pg^{\phi\phi}, \\ T^{tr} &= \rho h\frac{W^2}{\alpha}v^r. \end{aligned} \tag{18}$$

3.3. Geodesics flows

As a general relativistic test problem, the accretion of dust particles onto a black hole are solved. The exact solution for pressureless dust is given in Appendix A. This problem is numerically analyzed in 2D in spherical coordinates at constant $\theta = \pi/2$, which is the equatorial plane, so the spatial numerical domain is the (r, ϕ) plane. In this calculation, $2.4 \leqslant r \leqslant 20$ and $0 \leqslant \phi \leqslant 2\pi$ are used for the computational domain. The initial conditions for all variables are chosen to have negligible values except the outer boundary ($r = 20M$) where gas is continuously injected radially with the analytic density and velocity. Throughout the calculation, whenever values at the outer boundary are needed the analytic values are used. The code is run until a steady state solution is reached, using outflow boundary conditions at $r = 2.4$, inflow boundary conditions at $r = 20$ and the periodic boundary in the ϕ direction. It is found that the resulting numerical solution does not develop any angular dependence during the simulation.

In Fig. 1, the rest-mass density ρ, absolute velocity $v = (v^i v_i)^{1/2}$ and radial velocity v^r are plotted as a function of radial coordinate at a fixed angular

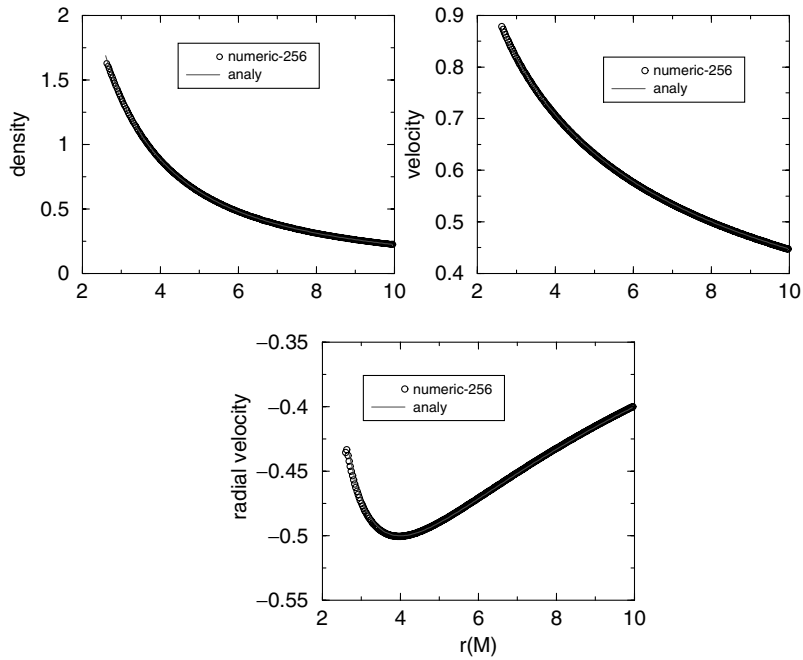

Fig. 1. The analytic solutions (red solid lines) with the numerical solutions (black circles) using 256 zones in the radial direction for thermodynamical variables, ρ, v, and v^r. (For interpretation of the references in color in this figure legend, the reader is referred to the web version of this article.)

Table 1
L_1 norm error and convergence factors are given for different resolutions

No. of points	No. of time step	L_1 norm error	Convergence factor
Convergence test			
32	1	1.675E−5	
64	2	4.0811E−6	4.105
128	4	9.6456E−7	4.23
256	8	2.1372E−7	4.51

position. The numerical solution agrees well with the analytic solution. The convergence test are also made on this problem to test the behavior of the source terms in the GR Hydro code. Some convergence tests with the SR Hydro code are conducted to confirm the second order convergent [6]. In this case, we are looking for convergence rate with source terms. The analytic values of the accretion problem are used as initial conditions, and the computational domain is chosen from $r_{\min} = 10M$ to $r_{\max} = 30M$. The convergence results are given in Table 1. It is noticed that code gives roughly second order convergence.

The conservation form of general relativistic hydrodynamical equations are solved. It is expected that conserved variables must be conserved to machine accuracy, $\sim 10^{-16}$. The checking the results of conservation variables in the numerical test problem shows that these variables conserved to machine accuracy.

In this part of same test problem, we do an AMR test. For uniform grid runs, the amount of time it takes to reach a steady state solution increases with resolution. We carried out a 3-level AMR calculation to compare with a uniform one for geodesic infall to see the behavior of AMR in this problem. In Fig. 2, we plot AMR and uniform runs on top of each other for density vs. radial Schwarzschild coordinate. We see that while the AMR solution has reached a steady state at $t = 151M$, the uniform solution has not reached a steady state by the same time.

3.4. Circular motion of test particles

We will now simulate the circular motion of a fluid with the numerical code. To do this we set up a circular flow with negligible pressure in the equatorial plane, in which angular velocity at each radial direction r is the Keplerian value, Eq. (B10). This is called a Keplerian. The last stable circular orbit for a particle moving around a Schwarzschild black hole is at $r = 6M$ (M is mass of black hole). Therefore, the gas or particles will fall into the black hole if their radial position is less than $6M$. When their radial position is bigger than $6M$, they should rotate in a circular orbit. Here we simulate this problem and

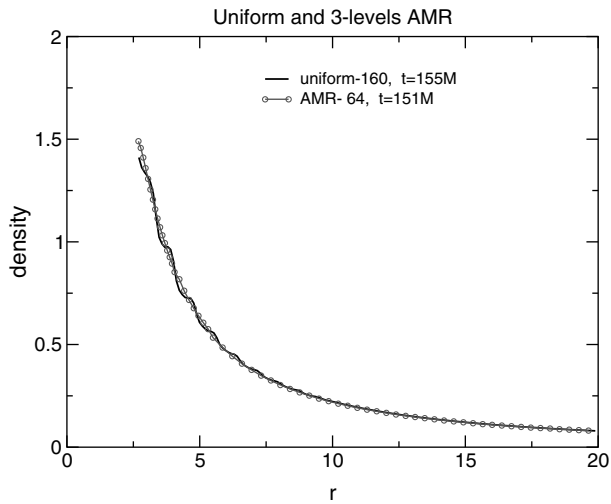

Fig. 2. The numerical solutions from a 3-level AMR run (64 zones, red circles) and a uniform grid run (160 zones, black straight line) for density vs. radial coordinate. (For interpretation of the references in color in this figure legend, the reader is referred to the web version of this article.)

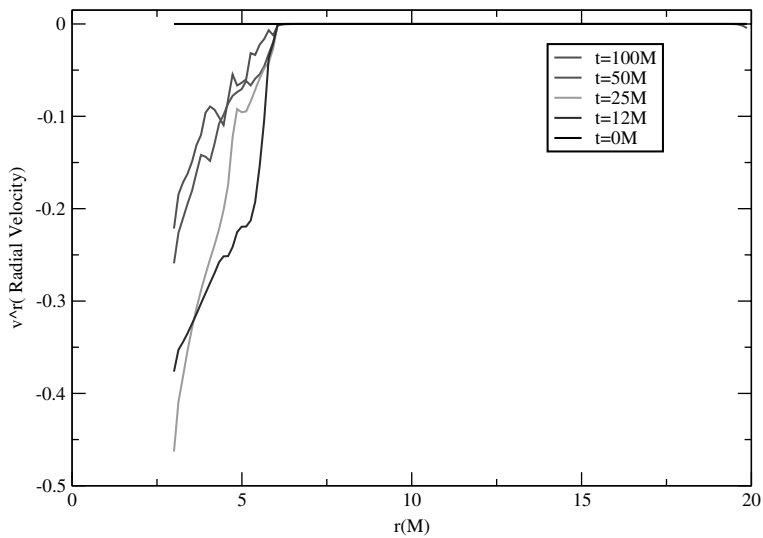

Fig. 3. Radial velocity vs. r is plotted. The radial velocity of fluid in the disk stays zero for $r > 6M$, during the evolution. $r = 6M$ is called the last stable circular orbit in a Keplerian disk.

compare the numerical solution with the analytic expectations. This problem tests the code with sources in the ϕ direction.

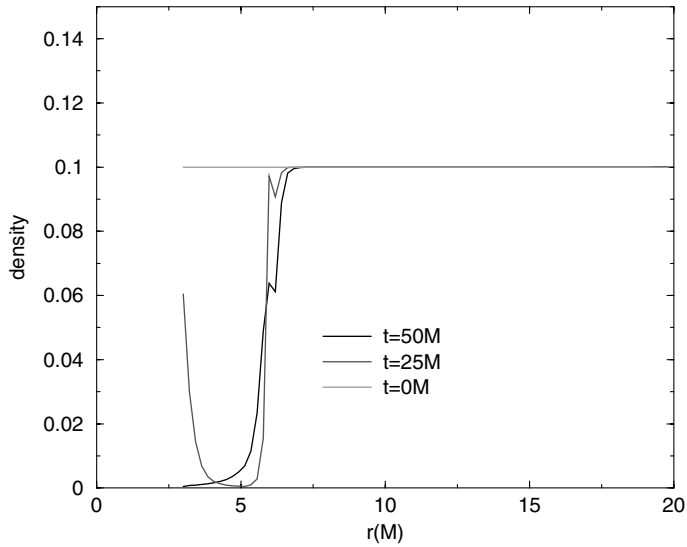

Fig. 4. Density vs. r is plotted. Density of the fluid is plotted at different times using different colors. The matter falls into the black hole while r is less than $6M$.

In order to simulate this problem, we chose the computational domain to be $3M \leqslant r \leqslant 20M$ and $0 \leqslant \phi \leqslant 2\pi$. The computational domain is filled with constant density and pressureless gas, rotating in circular orbits with the Keplerian velocity and zero radial velocity. In Fig. 3, the radial velocities of the gas vs. radial coordinate at different times are plotted. It is numerically observed that the gas inside the last stable orbit, $r = 6M$, falls into the black hole while gas outside the last stable orbit follows circular motion with the Keplerian velocity as we expect analytically. In Fig. 4, we plot the density of the fluid vs. radial coordinate at different times to see the behavior of the disk. It is clear from that gas falls into the black hole for $r < 6M$. So the numerical results from our code are consistent with the analytic expectations.

4. Numerical modeling of the accretion disks in the Schwarzschild coordinate

In the present work, we do not intend to make a very concrete model for particular object, and it is assumed to be a rather simple initial configuration of gas. At $t = 0$ computational domain filled with some negligible values for density and pressure with zero radial and angular velocity. The injected value from companion star from outer boundary of computational domain are: $\rho_{\text{in}} = 1.0$, $p_{\text{in}} = 10^{-3}/\gamma$, $v^r = 0.01$ and v^ϕ which is the Keplerian fluid velocity. Computational domain is $3M \leqslant r \leqslant 100M$ and $0 \leqslant \phi \leqslant 2\pi$, where M is the

mass of black hole. The following problems solved are 2D modeling on an equatorial plane.

The choice of boundary conditions at the inner and the outer numerical boundary is rather important. The boundary conditions are treated as follows. The fictitious cell is placed just outside of a boundary and we prescribe physical variables in the fictitious cell. Numerical fluxes on the boundary wall are computed by solving a Riemann problems between states. The following boundary conditions are used. The value of physical variables in the fictitious cells are the same as those in the neighboring interior cells at all times. Radial velocities direction can be changed depending on the inner or outer boundary condition used.

4.1. $\gamma = 1.05$

The first results of the spiral shock wave are given on the accretion disk around the black hole using the Schwarzschild metric. In all simulations, the black hole is at the center of computational domain and it is represented as a white hole in the graphics. First, gas is injected from the outer boundary to accrete an accretion disk with spiral shock wave and then the injection is stopped to see the behavior of accretion disk during the evolutions. Finally, the numerical simulation is stopped when solution reaches a steady state.

The density of the accretion disk is illustrated in Fig. 5 at $t = 19{,}643M$. In early time of simulation accretion disk is not in steady state yet but two-armed spiral shock is already created and dynamical structure of the disk is not changed any more. The only thing which changes during the simulation after the certain evolution time is the amplitude of density. It is also shown in Fig. 6 that the mass of accretion disk during the process of gas from the outer boundary by the companion star is in the steady states between the evolution times $10{,}000M$–$19{,}643M$. The two-armed spiral shock is created for the case $\gamma = 1.05$ during the injecting gas and also this spiral arms and accretion disk go to steady state.

In order to watch the behavior of the spiral shock on an accretion disk while no matter gets into accretion disk, the injected gas is stoped. It is numerically observed that initial structure of two-armed spiral shock wave is slightly changed because the hydrodynamical forces given by the shock, which is created by injected gas, is gone. In order to balance the forces on the accretion disk, the spiral shock waves are kept, which is more compact than the one in the beginning of this simulations, around the black hole. This newly formed two-armed spiral shocks are plotted at $t = 47{,}526M$ in Fig. 7. These shocks are in the steady state and two-arms spiral shock almost 180° apart to each other. In Fig. 8, we depict 1D cut at a fixed radial coordinate, $r = 20.12M$ for density, radial velocity, orbital velocity and pressure at $t = 47{,}526M$. Two-armed spiral shocks are clearly observed and they can be called strong shock. Angular

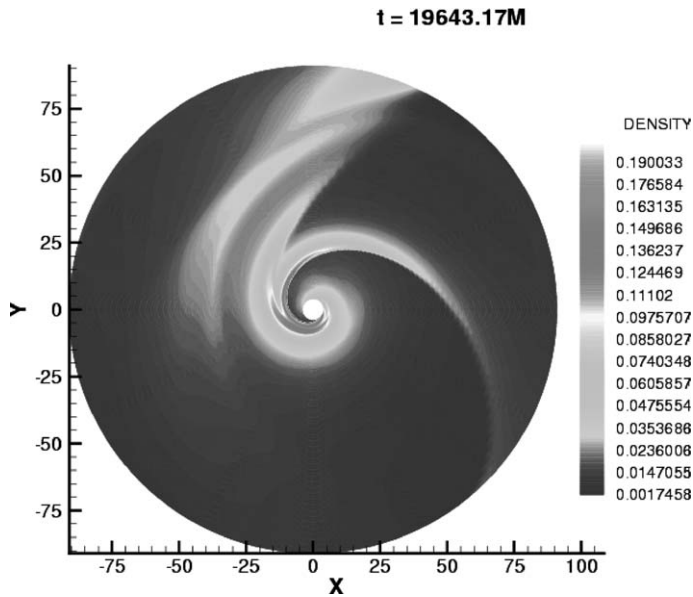

Fig. 5. Plotting the density in the r–ϕ plane with color for $\gamma = 1.05$. It is taken at $t = 19{,}643M$ and it is in steady state. Two-armed spiral shock wave is created.

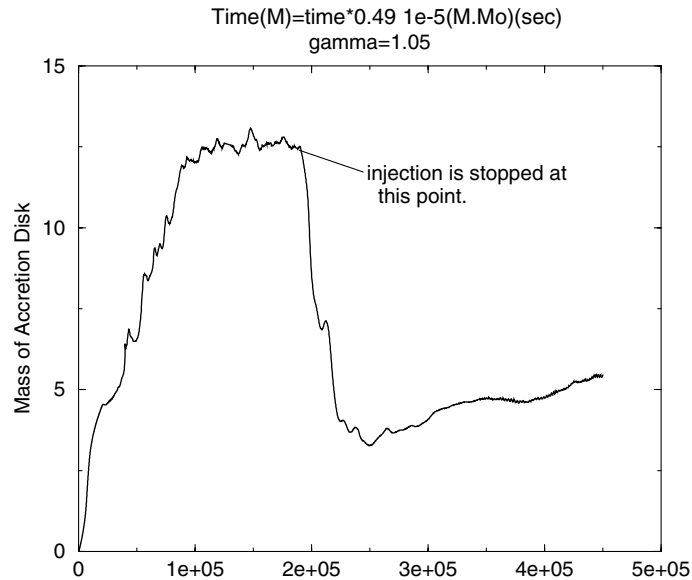

Fig. 6. Mass of accretion disk vs. time is plotted during the hole evolution. The injection is stopped at maximum mass.

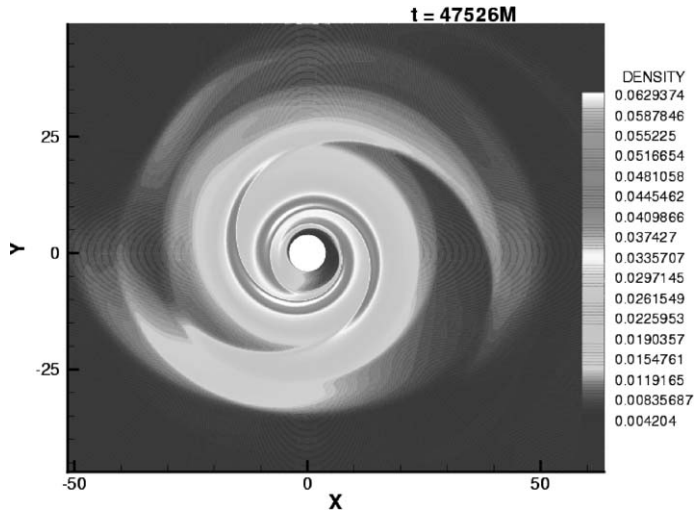

Fig. 7. Zooming the interesting part of accretion disk at $t = 47{,}526M$ to see two-armed shock wave clearly.

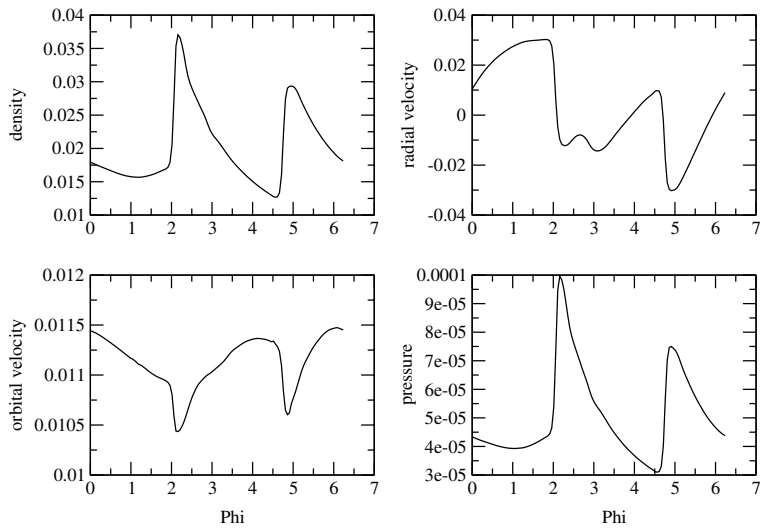

Fig. 8. Plotting the density, radial velocity, orbital velocity and pressure for accretion disk at $t = 47{,}526M$ in fixed $r = 20.12M$.

momentum transform is also seen in that graphic because the orbital velocities of spiral arms are less than the orbital velocity of accretion disk.

4.2. $\gamma = 1.2$

In this case, the same problem is solved for accretion disk except $\gamma = 1.2$ which is more expressible than the $\gamma = 1.05$. In order to accrete an accretion disk, the same injection is made from the outer boundary with the case of $\gamma = 1.05$ and numerical simulation is run until solution reach to a steady state. After all the injection is stoped, and the behavior of accretion disk, and spiral shock waves are numerically observed.

We do injection from outer boundary continuously to create an accretion disk around the black hole for $\gamma = 1.2$. In Fig. 9, the two-armed spiral shock waves are created. The solution is almost in steady state in Fig. 9. Even though the solution is not in steady state, the structure of accretion disk is not changed during the evolutions. The result for $\gamma = 1.2$ was comparable with Makita et al. [11]. But there are some differences around the black hole because our code fully relativistic and it can give detail structure when the matter close to black hole. Another difference in my code and Makita et al. [11] is that we use inflow boundary condition that is allowed to gas fall into black hole but they use freezing boundary. Using a different boundary close to black hole also makes big difference in the structure of spiral shock waves.

In order to understand how the spiral arms behave after companion star is removed, the injecting gas from the outer boundary is stoped. After the

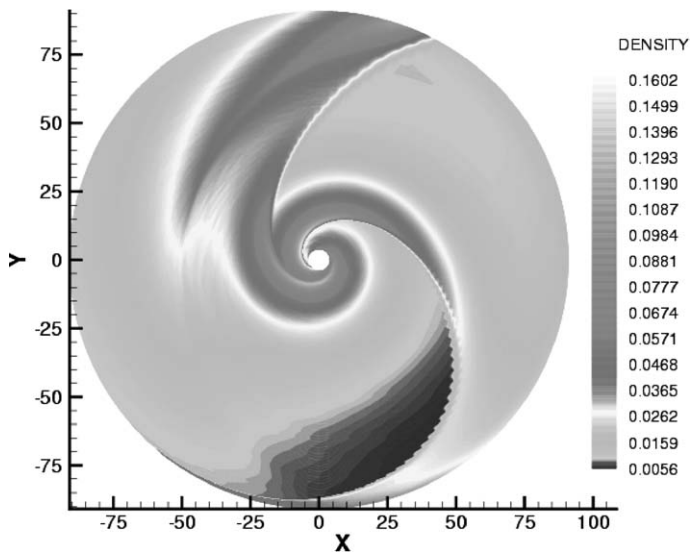

Fig. 9. Plotting the density in the r–ϕ plane with color for $\gamma = 1.2$. It is taken at $t = 17{,}502M$. It is in the steady state and two-armed spiral shock wave is already created and the structure of disk does not change.

Fig. 10. Plotting the density in the r–ϕ plane with color for $\gamma = 1.2$. It is taken at $t = 19{,}475M$ after injected is stopped at $t = 17{,}502M$. It is seen that two-armed spiral shock wave is still kept because they are created tidal forces on the accretion disk.

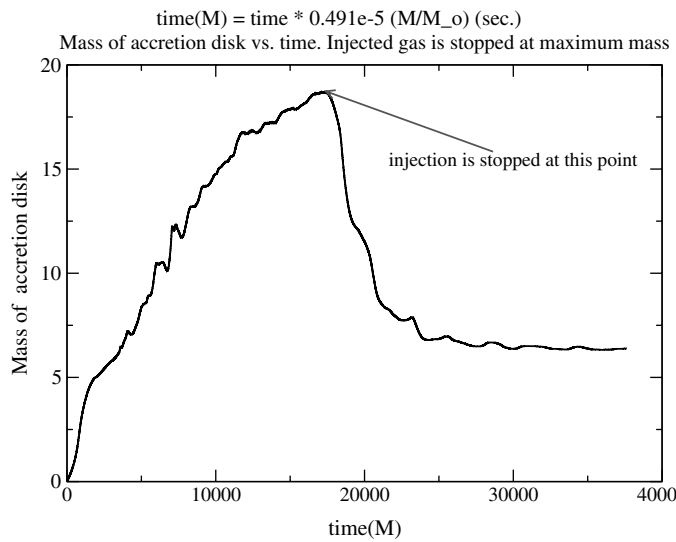

Fig. 11. Mass of accretion disk vs. time is plotted during the hole evolution. The injection is stopped at maximum mass.

injecting is not allowed any more at $t = 17{,}502M$, Fig. 10 displays numerical result at $t = 19{,}475M$ that two-armed spiral shock waves are still kept because of tidal forces between companion star and black hole. Mass of the accretion during the whole process is given in Fig. 11. It reaches a maximum mass, which is almost called a steady-state point, whenever the companion star is removed, mass of accretion disk starts to decrease and goes to steady-state point. That point has also two-armed spiral shock waves.

5. Conclusion

The angular momentum loss of gas in the accretion disk in a close binary system is one of the very important phenomena in the astrophysics. The most accepted model that explains the mechanism of angular momentum transport is alpha disk model. An alternative model that needs no viscosity for angular momentum transfer is the spiral shock waves on an accretion disk which are an important mechanism to transform the angular momentum. In this simulation, it is concluded that accretion disk is rotating with sub-Keplerian velocity, which is carrying positive angular momentum, and spiral shock waves moving much slower than the disk and they are carrying the negative angular momentum. When the disk material hits the spiral wave, the angular momentum of accretion disk is transformed to out of accretion disk. The shock waves around the black hole are a mechanism of transforming gravitational energy to radiation energy which is observed by the different X-ray observatory satellite, such as Chandra.

Spiral arms in an accretion disk are one of the mechanism to emit X-ray. We have looked at the spiral structure, which is created at around the black hole when the matter falls from the companion star to primary star. Spiral structure in an accretion disk is created under certain condition. To create spiral arms, adiabatic index must be less or equal than 1.2.

In these simulations, three different simulations are done for $\gamma = 1.1$, 1.2 and 5/3. These simulations show that we do not have any spiral arms for $\gamma = 5/3$ (the graphic for his case did not put here) but for the others. These results are consistent with results from Makita et al. [11]. We have also watched the behavior of accretion disk after companion star stop injection. The two-armed spiral structure kept during the evolution. It concludes that the spiral shocks are formed by tidal forces, not by the inflow, of which claim was posed by Bisikalo et al. [1].

From the point of view of dependence γ, it is concluded that spiral arms are more tightly in smaller γ cases than larger ones. Lower γ means cooler disk with larger Mach number of the flow. Our results are comparable with those of Makita et al. [11] who solve Newtonian hydrodynamical equation. Ours and their results also agree while adiabatic index, γ, is bigger than 1.2, two-armed

spiral shock wave is not created which is observed for $\gamma = 5/3$. Even the accretion disk may not be formed.

The numerical simulations of general relativistic hydrodynamic equations gives more detailed structure inside the $10M$. The location of inner radius of spiral shock waves depend on adiabatic index. We saw that when the spiral shock waves created, the inner radius of shock waves attached to the inner boundary, $3M$ which is close to the event horizon. Around this region Mach number is bigger and so gravity is always dominant.

Our future studies will focus on the numerical simulation of the spiral structure on an accretion disk around the Kerr black hole. This problem can be set up replacing Kerr matrix instead of Schwarzschild matrix.

Acknowledgments

I would like to thank Joan M. Centrella, Cole Miller, Demos Kazanas and Tod Strohmayer for useful discussions. This project was carried out at NASA/GSFC, Laboratory of High Energy Astrophysics. It is supported by NASA/GSFC IR&D. It has been performed using NASA super computers/T3E clusters.

Appendix A. The analytic solution of geodesics flows

Pressureless gas, also called dust, falling onto a black hole in the radial direction is called geodesic flow. It can be also called free falling gas because there are no pressure forces opposing the inward motion of the gas.

We use the fact that the elements of the accreting fluid fall along geodesics to get the analytic solution. In axisymmetric steady-state flows, the binding energy per baryon hU_t is conserved. Hence for dust particles, $h = 1$ and the gravitational binding energy U_t will remain constant. Since $U^\mu U_\mu = -1$, $v^r(r)$ is now determined in terms of input a constant U_t and the known metric functions. Note that $U_\theta = U_\phi = 0$.

First, we start with the geodesic equation for free falling dust:

$$\begin{aligned} &\nabla_{\vec{u}}\vec{U} = 0, \\ &U^\alpha_{;\beta}U^\beta = (U^\alpha_{,\beta} + \Gamma^\alpha_{\gamma\beta}U^\gamma)U^\beta = 0. \end{aligned} \tag{A1}$$

Eq. (A1) can be rewritten using $U^\alpha = \mathrm{d}x^\alpha/\mathrm{d}\lambda$,

$$\frac{\mathrm{d}U^\alpha}{\mathrm{d}\lambda} + \Gamma^\alpha_{\gamma\beta}U^\gamma U^\beta = 0. \tag{A2}$$

Substituting the index $\alpha = 0 = t$ in Eq. (A2) gives

$$\frac{\mathrm{d}U^t}{\mathrm{d}\lambda} + \Gamma^t_{\gamma\beta} U^\gamma U^\beta = 0. \tag{A3}$$

Most of the Christoffel symbols at Eq. (A3) are zero, except $\Gamma^t_{tr} = \Gamma^t_{rt} = \frac{1}{2} g^{tt} \partial_r g_{tt} = \frac{1}{2}(2M/(r(r-2M)))$. Substituting the non-zero Christoffel symbols into Eq. (A3) gives us

$$\frac{\mathrm{d}U^t}{\mathrm{d}r} = -\frac{2M}{r(r-2M)} U^t, \tag{A4}$$

where $\mathrm{d}U^t/\mathrm{d}\lambda = (\mathrm{d}U^t/\mathrm{d}r)(\mathrm{d}r/\mathrm{d}\lambda)$.

After doing some straightforward integration, Eq. (A4) goes to

$$U^t = \frac{1}{\left(1 - \frac{2M}{r}\right)}. \tag{A5}$$

To compute the radial component of the fluid velocity of geodesic gas, we need to know the radial four velocity of the gas. In order to compute that, we use the normalization of four velocities, which is

$$\begin{aligned} &U^\mu U_\mu = -1, \\ &U^t \gamma_{tt} U^t + U^r \gamma_{rr} \gamma^r = -1. \end{aligned} \tag{A6}$$

We substitute Eq. (A5) into Eq. (A6), to

$$U^r = \sqrt{\frac{2M}{r}}. \tag{A7}$$

Using the relations between the four and three velocities, $U^r = W v^r$, $U^t = W/\sqrt{1-(2M/r)}$, we get

$$v^r = \sqrt{\frac{2M}{r}} \sqrt{1 - \frac{2M}{r}}, \tag{A8}$$

where v^r is the velocity which is observed by an observer outside the horizon.

Now, we compute the density using the continuity equation from Eq. (5) which is

$$\partial_t(\sqrt{\gamma} W \rho) + \partial_i(\alpha v^r D) = 0. \tag{A9}$$

Since we are looking for a steady state solution the time derivative of variables is zero and we have only the radial derivative in Eq. (A9). Then, the density equation becomes

$$\partial_i(\alpha v^r D) = 0. \tag{A10}$$

After doing integration of Eq. (A10), we get

$$\alpha v^r D = d, \tag{A11}$$

where d is an integration constant. Now D can be computed from Eqs. (A8) and (A11),

$$D = \frac{d}{\left(1-\frac{2M}{r}\right)\left(\frac{2M}{r}\right)^{\frac{1}{2}}}. \tag{A12}$$

Finally, we compute the density ρ from Eqs. (A8) and (A12)

$$\rho = \frac{1}{W}\frac{d}{r^2\left(\frac{2M}{r}\right)^{\frac{1}{2}}\left(1-\frac{2M}{r}\right)^{\frac{1}{2}}}, \tag{A13}$$

where W is the Lorentz factor and given by

$$W = \frac{1}{\left(1-\frac{2M}{r}\right)^{\frac{1}{2}}}. \tag{A14}$$

Appendix B. The analytic representation of circular motion of a test particle

In this appendix, we compute the angular velocity and circular velocity of a particle on a circular orbit in the Schwarzschild spacetime, analytically.

Since Schwarzschild geometry is time independent and spherically symmetric, the conserved quantities can be determined by the trajectory of particles. Because of spherical symmetry, motion is always defined at a single plane and we can chose this plane to be the equatorial plane ($\theta = \pi/2$). Then θ is constant in that plane for the motion of particles and the θ derivatives vanish. The components of the momentum [14] are

$$\begin{aligned} p^t &= g^{tt}p_t = \frac{mE}{\left(1-\frac{2M}{r}\right)}, \\ p^r &= m\frac{\mathrm{d}r}{\mathrm{d}\tau}, \\ p^\theta &= 0, \\ p^\phi &= g^{\phi\phi}p_\phi = \frac{mL}{r^2}, \end{aligned} \tag{B1}$$

where m, E , τ and L are the mass of particle, total energy, proper time and angular momentum, respectively. Here $E = -p_t/m$ and $L = p_\phi/m$.

Now, we can derive the equation of motion for a particle in the equatorial plane using Eq. (B1) and the conservation relation, $\vec{p}\cdot\vec{p} = -m^2$. This gives us

$$\left(\frac{\mathrm{d}r}{\mathrm{d}\tau}\right)^2 = E^2 - \left(1-\frac{2M}{r}\right)\left(1+\frac{L^2}{r^2}\right). \tag{B2}$$

Eq. (B2) can be rewritten by defining an effective potential $V(r)$ and we get

$$\left(\frac{dr}{d\tau}\right)^2 = E^2 - V^2(r), \tag{B3}$$

where $V^2(r) = (1 - \frac{2M}{r})(1 + \frac{L^2}{r^2})$. Eq. (B3) implies that since the left side of that equation is positive or zero, the total energy of a trajectory can be bigger or equal to the effective potential.

In order to compute the angular velocity and period of a particle in a circular orbit, we differentiate Eq. (B3) with respect to τ, and get

$$\frac{d^2r}{d\tau^2} = -\frac{1}{2}\frac{dV^2(r)}{dr}. \tag{B4}$$

It is clear from Eq. (B4) that a circular orbit, which has constant r, is possible only at a minimum or maximum of the effective potential, $V^2(r)$. In a circular orbit r is constant and the left side of Eq. (B4) goes to zero. If we take $d^2r/d\tau^2 = 0$ and substitute in the expression for the effective potential, we can compute the circular orbit radius as

$$r = \frac{L^2}{2M}\left(1 \pm \sqrt{\left(1 - \frac{12M^2}{L^2}\right)}\right). \tag{B5}$$

From Eq. (B5), a stable circular orbit at radius r has angular momentum which is

$$L^2 = \frac{Mr}{1 - \frac{3M}{r}}. \tag{B6}$$

The total energy in a circular orbit is $E^2 = V^2$ and it is

$$E = \left(1 - \frac{2M}{r}\right)^2 \Big/ \left(1 - \frac{3M}{r}\right). \tag{B7}$$

Now, the non-zero components of the four velocity of a particle in the plane are

$$\frac{d\phi}{d\tau} = U^\phi = \frac{P^\phi}{m} = g^{\phi\phi}\frac{P_\phi}{m} = g^{\phi\phi}L = \frac{L}{r^2} \tag{B8}$$

and

$$\frac{dt}{d\tau} = U^t = \frac{P^t}{m} = g^{tt}\frac{P_t}{m} = g^{tt}(-E) = \frac{E}{1 - \frac{2M}{r}}. \tag{B9}$$

We find the angular velocity by dividing Eq. (B8) by Eq. (B9):

$$\frac{d\phi}{dt} = \frac{d\phi/d\tau}{dt/d\tau} = \sqrt{\frac{M}{r^3}}; \tag{B10}$$

this is called the Keplerian angular velocity.

Finally, we can compute the circular velocity of a particle using the definition of four velocity relativistic hydrodynamical equations given in Section 2, Eqs. (B8) and (B9). We get

$$v^{\phi} = \frac{1}{\alpha}\frac{U^{\phi}}{U^{t}},$$
$$v^{\phi} = \frac{1}{\sqrt{(1-\frac{2M}{r})}}\sqrt{\frac{M}{r^3}}. \tag{B11}$$

References

[1] D.V. Bisikalo, A.A. Boyarchuk, V.M. Chechetin, O.A. Kuznetsov, D. Molteni, MNRAS (1998).
[2] S.K. Chakabarti, D. Molteni, Astrophys. J. 417 (1993) 671–676.
[3] S.K. Chakabarti, Astrophys. J. 484 (1997) 313–322.
[4] R. Dgani, M. Livio, O. Regev, Astrophys. J. 436 (1994) 270.
[5] R. Donat, J.A. Font, J.M. Ibanez, A. Marquina, J. Comput. Phys. 146 (1998) 58.
[6] O. Dönmez, Astrophys. Space Sci. 293 (2004) 323–354.
[7] J.A. Font, M. Miller, W.-M. Suen, M. Tobias, Phys. Rev. D 61 (2000) 044011.
[8] P. Godon, Astrophys. J. 480 (1997) 329.
[9] J.F. Hawley, L. Smarr, J.R. Wilson, Astrophys. J. 277 (1985) 296–311.
[10] G. Lanzafame, D. Molteni, S.K. Chakabarti, Mon. Not. R. Astron. Soc. 299 (1998) 799–804.
[11] M. Makita, K. Miyawaki, T. Matsuda, Mon. Not. R. Astron. Soc. 000 (2000) 1, 13.
[12] D. Molteni, G. Toth, O.A. Kuznetsov, Astrophys. J. 516 (1999) 411–419.
[13] M. Rozyczka, H.C. Spruit, Astrophys. J. 417 (1993) 677.
[14] B.F. Schutz, in: B.F. Schutz (Ed.), A First Course in General Relativity, Cambridge University Press, Cambridge, 1985.
[15] D. Steeghs, E.T. Harlaftis, K. Horne, MNRAS 209 (1997) L28.